Femtosecond laser nanoablation of glass in the near-field of single wall carbon nanotube bundles

2008 J. Phys. D: Appl. Phys. 41 185306

(http://iopscience.iop.org/0022-3727/41/18/185306)

IOP PUBLISHING JOURNAL OF PHYSICS D: APPLIED PHYSICS

J. Phys. D: Appl. Phys. **41** (2008) 185306 (7pp) doi:10.1088/0022-3727/41/18/185306

Femtosecond laser nanoablation of glass in the near-field of single wall carbon nanotube bundles

Samuel X Guo and Adela Ben-Yakar[1]

Mechanical Engineering Department, University of Texas at Austin, 1 University Station C2200, Austin, TX 78712, USA

E-mail: ben-yakar@mail.utexas.edu

Received 3 June 2008, in final form 14 July 2008
Published 29 August 2008
Online at stacks.iop.org/JPhysD/41/185306

Abstract

This paper presents an experimental study on the femtosecond (fs) laser ablation of bundles of single wall carbon nanotubes (SWCNTs) deposited on glass and the resulting nanoablation of glass beneath the bundles. The peak ablation threshold of SWCNT bundles is $50 \pm 12\,\mathrm{mJ\,cm^{-2}}$, which is about ten times lower than the theoretical ablation threshold of individual SWCNTs. Nanoscale ablation of the glass surface (30–50 nm wide, 20–50 nm deep and micrometres long) directly beneath the bundles is possible at a laser fluence of $920 \pm 76\,\mathrm{mJ\,cm^{-2}}$, which is 4–5 times lower than the fs laser ablation threshold of glass. We attribute these reduced ablation thresholds to the enhancement of fs laser pulses in the near-field of nanotube bundles. This nanoablation approach can be used for lithographical and surgical applications requiring nanoscale precision.

1. Introduction

Laser ablation using ultrafast laser pulses below tens of picoseconds has been extensively studied for precise ablation of various materials [1–3]. During interaction with dielectric materials, for example, ultrafast pulses provide high peak intensities that can initiate nonlinear processes, such as multiphoton, avalanche and tunnelling ionizations [4]. These nonlinear processes result in reduced ablation thresholds that are especially critical when interacting with high bandgap, sensitive materials, such as glass and biological tissue [5]. In contrast to long pulse ablation, which is inherently dominated by the thermal diffusion process, ultrafast laser ablation minimizes the heat affected zone (HAZ) and correspondingly allows material removal with high precision.

Single wall carbon nanotubes (SWCNTs) are of practical interest since they can potentially be used in many applications, such as chemical sensors and electronic devices [6–8]. Recently, SWCNTs have attracted significant research attention in biological and medical areas [9–14]. Of particular interest, Kam *et al* [14] and Panchapakesan *et al* [12] have proposed a new class of techniques for cancer therapy using SWCNTs' strong absorption of light at near infrared (NIR) wavelengths and transferring heat from incident laser light to SWCNTs which have been either loosely adsorbed onto or delivered into cancer cells. Strong NIR light absorption at the plasmonic frequency by metallic nanostructures, such as nanorods [15] and nanoshells [16], has also been used for photothermal cancer therapy [17, 18]. The nanostructures act as efficient photothermal absorbers to locally destroy cancer cells at low laser energies [19]. To minimize the simultaneous destruction of neighbouring healthy cells, ultrafast laser pulses at NIR wavelengths could be used as a precise submicrometre surgical tool because of their small HAZ [5]. The interaction of ultrafast laser pulses with nanostructured materials such as gold nanoparticles16 or SWCNTs will provide local near-field enhancement of electromagnetic field and can be used to increase the precision by confining the ablation into nanodomains. However, so far the response of SWCNTs to ultrafast laser pulses in terms of ablation threshold and near-field enhancement has not been studied extensively.

While the interaction of ultrafast laser pulses with carbon materials such as graphite and diamond has been studied both theoretically and experimentally [20–24], their interaction with SWCNTs was explored only by a small number of studies [25–29]. Corio *et al* [25] and Ma *et al* [26], for

[1] Author to whom any correspondence should be addressed.

example, experimentally studied changes in the morphology and molecular structure of SWCNTs heated by a continuous wave laser. Romero *et al* performed computational analysis to eliminate defects in carbon nanotubes with femtosecond (fs) laser pulses [27]. Recently, Dumitrica *et al* calculated that the threshold for fs-laser fragmentation of SWCNTs is 2.8 eV atom^{-1}, corresponding to a peak laser fluence of about 0.48 J cm^{-2} [28]. Kocabas *et al* conducted multiple-shot picosecond laser ablation of SWCNTs to generate aligned arrays of carbon nanotubes [29]. They came to the conclusion that irradiation of SWCNTs with multiple picosecond pulses resulted in the accumulation of heat and subsequent thermal ablation of the nanotubes. In addition, Corio *et al* [25] found that single SWCNTs of small diameter are ablated at a lower threshold than those of larger diameter as a result of continuous wave laser-induced heating. However, the heat-diffusion based ablation using CW-laser irradiation or long duration laser pulses is fundamentally different from that with fs laser pulses, which is dominated by non-thermal mechanisms [3].

In this paper we study non-thermal ablation of CNTs using a single fs-laser pulse. We report the threshold of single-shot fs-laser ablation of SWCNT bundles on a glass substrate and the resulting nanoablation of glass beneath the bundles. Atomic force microscopy (AFM) is used to image a laser exposed area before and after ablation. Remarkably, nanoscale lines of 30–50 nm widths and 20–50 nm depths are generated on the glass substrate. Nanoablation is believed to be due to enhancement of laser pulses in the near field of the SWCNT bundles.

2. Experimental approach

Purified SWCNTs manufactured by the high pressure CO process were provided by Carbon Nanotechnologies Inc. (Houston, TX) with less than 15% ash content by weight. The as-received SWCNTs were further purified using modified oxidation and ultrasonication processes [30, 31]. Specifically, SWCNTs were oxidized in a box furnace for 14 h at 275 °C, followed by reflux in 2.5 M HNO_3 for 36 h. The resulting mixture was filtered through a 100 nm pore size polycarbonate filter, rinsed and re-suspended in N,N-dimethylmethanamide (DMF). Ultrasonication of the SWCNT/DMF mixture at a concentration of ∼50 mg L^{-1} for 2 h was performed to cut the SWCNTs into shorter lengths to promote their separation. Centrifugation (5000 rpm, 45 min) was used to remove larger impurities from the solution. The transmission electron microscope (TEM) image in figure 1 shows that the SWCNTs remain in a bundle state due to a substantial van der Waals attraction (∼950 meV nm^{-1}) [32]. The diameter of the bundles varies between 5 and 25 nm. A 2 μL aqueous sample of SWCNT suspension was deposited onto a glass wafer, which was subsequently heated to 120 °C for 20 min on a hot plate to evaporate DMF. Consequently, only a single layer of randomly distributed SWCNTs was left on the wafer. The density of SWCNTs on the glass wafer could be adjusted by the amount of solution deposited. We used borosilicate glass wafers with a surface roughness of less than 1 nm from Precision Glass and Optics (Santa Ana, CA). The wafers were ultrasonically cleaned with methanol prior to use.

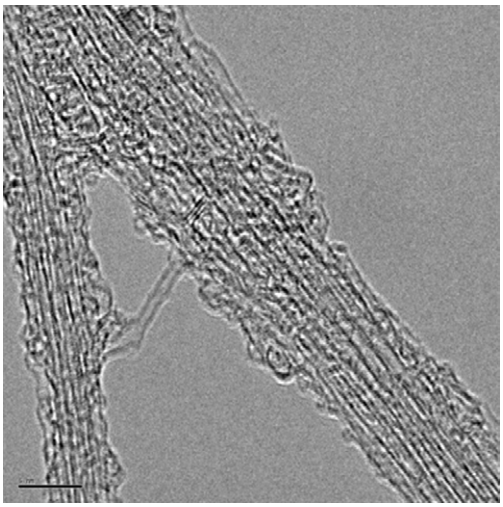

Figure 1. TEM image of SWCNT bundles after oxidation and ultrasonication processes. Scale bar is 5 nm.

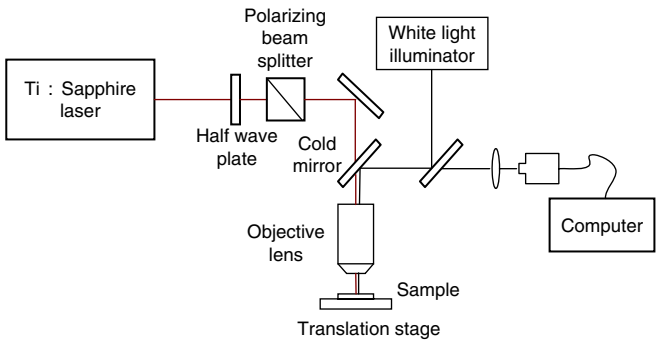

Figure 2. Schematics of the experimental setup.

Figure 2 illustrates the experimental setup. The laser pulses of 220 fs duration and 780 nm centre wavelength were generated using a regeneratively amplified Ti : sapphire laser (Spitfire, Spectra Physics, Mountain View, CA) at a 1 kHz repetition rate. The glass wafer surface was placed normal to the incident laser beam. The laser beam was linearly polarized and focused with a long working distance objective lens (Mitutoya, 10×, NA = 0.28) onto the glass wafer. The $1/e^2$ radius of the laser beam on the glass was $w_0 = 3.5 \pm 0.2\,\mu$m as measured using a previously published method [1]. The laser energy was adjusted by a combination of a polarizing cube beam splitter and a half wave plate and measured by a laser pulse energy meter (PD10, Ophir). The SWCNTs were imaged before and after laser ablation with an AFM (Digital Instruments Dimension 3000 scanning probe microscope) in tapping mode.

3. Results

To determine the laser ablation threshold of SWCNTs, we measured the minimum local laser fluence where SWCNTs started to disappear. Based on a Gaussian spatial profile of

the laser beam with a $1/e^2$ laser beam radius w_0, the radial distribution of laser fluence is presented by

$$F(r) = F_0^{\text{peak}} \exp\left(-\frac{2r^2}{w_0^2}\right), \quad (1)$$

where F_0^{peak} is the laser peak fluence and r is the distance from the centre of the beam. The laser pulse energy E, measured by the laser pulse energy meter, is related to the peak fluence by

$$F_0^{\text{peak}} = \frac{2E}{\pi w_0^2}. \quad (2)$$

For the measured radius of disappearance of SWCNTs r_0, the local ablation threshold fluence (peak fluence), $F_{\text{th}}^{\text{peak}}(r_0)$, is given by

$$F_{\text{th}}^{\text{peak}}(r_0) = \frac{2E}{\pi w_0^2} \exp\left(-\frac{2r_0^2}{w_0^2}\right). \quad (3)$$

In the literature, on the other hand, most studies report the fluence in terms of an average value defined by

$$F_0^{\text{ave}} = \frac{E}{\pi w_0^2}. \quad (4)$$

For consistency with our measurements we cite the data from the literature in terms of peak fluences.

Figures 3(*a*) and (*b*) show AFM images of SWCNTs on a glass substrate before and after irradiation with a single laser pulse at a peak fluence of 5.6 J cm^{-2}. Using fluences slightly above the glass ablation threshold of 5.2 J cm^{-2} [1], we could minimize debris due to ablation and prevent impairing the AFM imaging. Figure 3(*c*) shows the cross-sectional profile of the deposited carbon nanotubes before ablation and reveals that most tubes were bundled together with a diameter of 5–25 nm (see also figure 1). There are about 30 SWCNT bundles per 10 μm^2 area and the average bundle length is about 2 μm. The arrow in figure 3(*b*) indicates the direction of the laser polarization. The centre of the laser beam is represented by the cross of two perpendicular lines. The corresponding Gaussian distribution of the laser fluence is plotted in figure 3(*d*).

Three distinguished regions of ablation can be observed in figure 3(*b*). Concentric white circles are drawn to indicate the boundaries of these regions. The large circle (No 1) indicates the region where most carbon nanotubes are ablated, the medium circle (No 2) indicates the region where nano-width lines are ablated on glass, and the small circle (No 3) indicates the region where fs-laser ablation of glass at the microscale is observed. The radius r_0 of SWCNTs' disappearance indicated by the large white circle (No 1) is 5.35 μm, corresponding to a threshold fluence of $F_{\text{th}}^{\text{peak}}(r_0) = 52$ mJ cm^{-2} for SWCNTs' ablation.

To analyse the details of the region of glass nanoablation we present higher magnification AFM images in figure 4. A few elliptical and rectangular dotted shapes are added in the AFM images to highlight the regions of glass nanoablation before and after laser exposure. We observed that the glass nanoablation seen in figure 4(*b*) took place at the same exact positions of carbon nanotubes in figure 4(*a*). These nanolines on glass have a similar orientation and length of the carbon nanotubes that previously occupied those locations. The cross-sectional profiles along A–B and A′–B′ before and after ablation plotted in figure 4(*c*) clearly demonstrate that nanoablation occurs on glass directly beneath SWCNTs. The width of the nanoablated lines is between 30 and 50 nm and the depth is up to 50 nm. At the centre of the laser beam inside the small circle, we observe direct fs-laser ablation of glass up to a radius of 1.1 μm. This radius corresponds to a threshold fluence of 4.6 J cm^{-2} which is close to the published threshold of glass ablation of 5.2 J cm^{-2} [1]. The circular distribution of the nanoablation region allows us to estimate its threshold fluence. The measured distance from the centre of the laser beam is ∼3.6 μm, corresponding to a fluence of 840 mJ cm^{-2}. This fluence is about six times lower than the expected threshold of glass ablation.

To estimate the ablation thresholds, additional experiments were performed for a variety of laser fluences ranging from 0.2 to 3.5 J cm^{-2}. At fluences as low as 2.24 J cm^{-2}, direct fs-laser ablation of glass could not be observed anymore whereas nanoablation of glass could still be obtained. We analysed the laser exposed regions using AFM and measured the radius of circles indicating the disappearance of carbon nanotubes, the border of the nanoablated regions (nanolines) on glass and the border of fs-laser ablated craters on glass. By recognizing that material cannot be ablated at laser fluences lower than the threshold, namely, $r = 0$ when $F_0^{\text{peak}} = F_{\text{th}}^{\text{peak}}$, equation (1) yields

$$r^2 = \frac{w_0^2}{2} \ln\left(\frac{F_0^{\text{peak}}}{F_{\text{th}}^{\text{peak}}}\right). \quad (5)$$

Figure 5 presents the measured radius data as a function of the peak fluence, F_0^{peak}. Linear fits to data points based on equation (5) reveal the linear relationship between the squared radius of the ablated region and the logarithm of the incident laser fluence. The extrapolation of the linear fit to $r^2 = 0$ results in threshold fluences, $F_{\text{th}}^{\text{peak}}$, for fs-laser ablation of glass, nanoablation of glass and ablation of SWCNT bundles of 4.1 ± 0.2 J cm^{-2}, 920 ± 76 mJ cm^{-2} and 50 ± 12 mJ cm^{-2}, respectively. Our measured ablation threshold of SWCNT bundles is about ten times lower than the theoretically calculated value (about 480 mJ cm^{-2}) for the ablation of individual (not bundled) SWCNTs [28]. The reason for this discrepancy might be due to the fact that the theoretical value for individual SWCNT was computed based on the estimated data for graphite. Their calculated threshold fluence for individual SWCNTs is indeed similar to that for graphite (500 mJ cm^{-2}) [33]. On the other hand, it is also possible that these lower values of measured ablation thresholds of bundled SWCNTs are a result of a possible near-field enhancement between the bundled nanotubes.

4. Discussion

Notably, the threshold fluence for glass nanoablation (0.92 J cm^{-2}) is about 4.5 times smaller than the measured

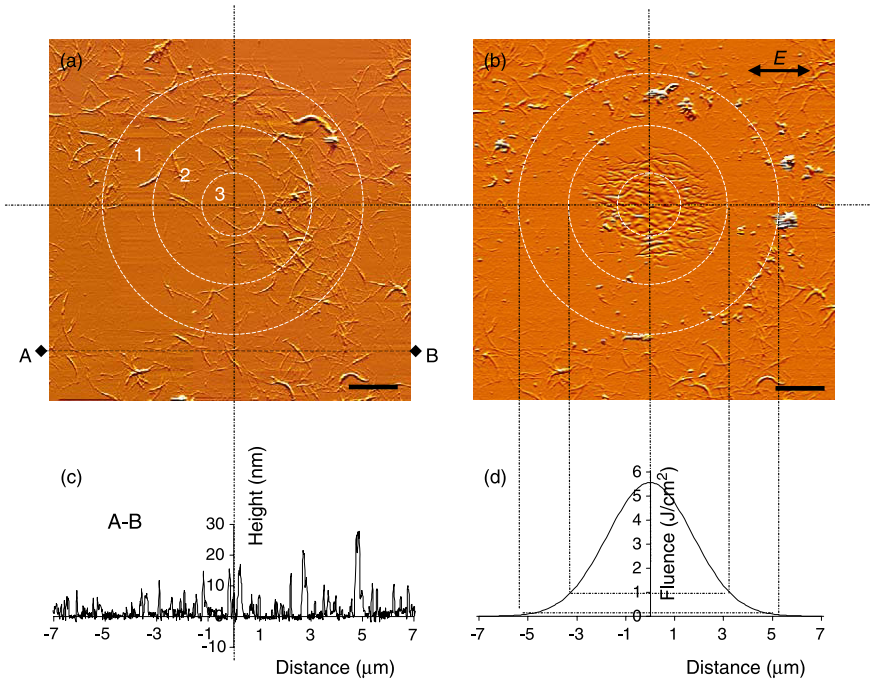

Figure 3. AFM images of SWCNTs deposited on the glass substrate before (*a*) and after (*b*) fs-laser pulse irradiation. The area within the large circle indicates the region where SWCNTs disappeared. Glass ablation at the nanoscale and microscale takes place within the smaller circles, Nos 2 and 3, respectively. The corresponding distribution of the local laser fluence is plotted in the Gaussian curve in (*d*). The cross-sectional profile along A–B is plotted in (*c*). Scale bars are 2 μm.

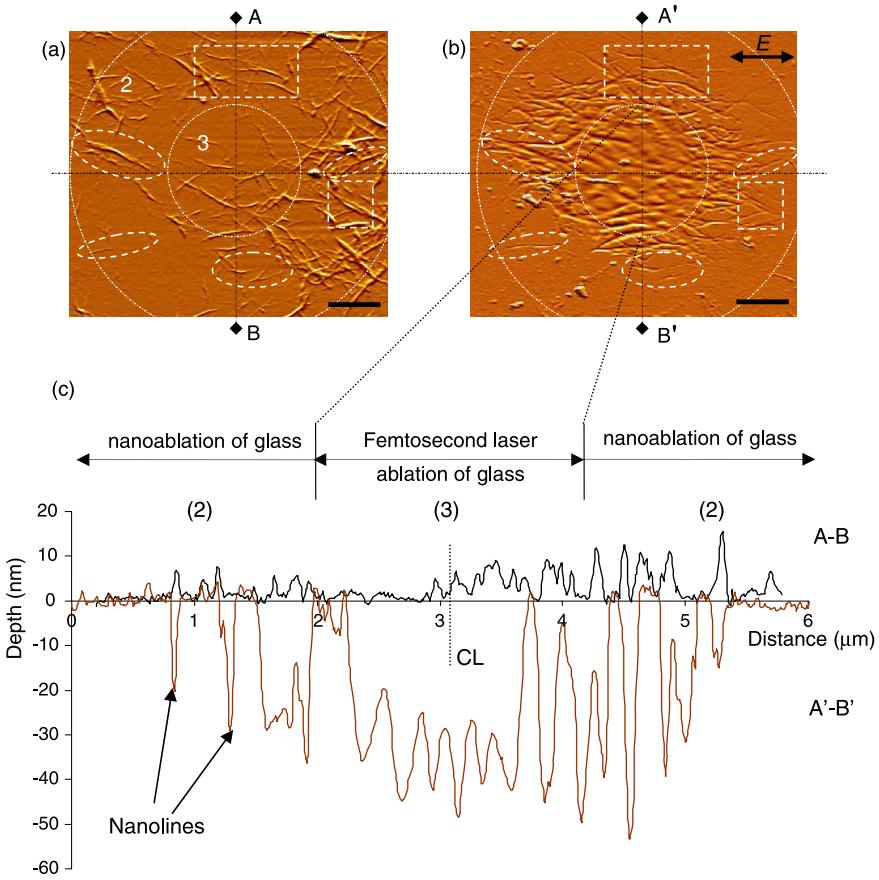

Figure 4. Magnified AFM images of the region within two small circles presented in figure 3 before (*a*) and after (*b*) ablation. Several dotted ellipses and rectangles are drawn to highlight that nanolines are directly created beneath the SWCNTs. Scale bars are 1 μm. (*c*) The cross-sectional profiles along A–B and A′–B′.

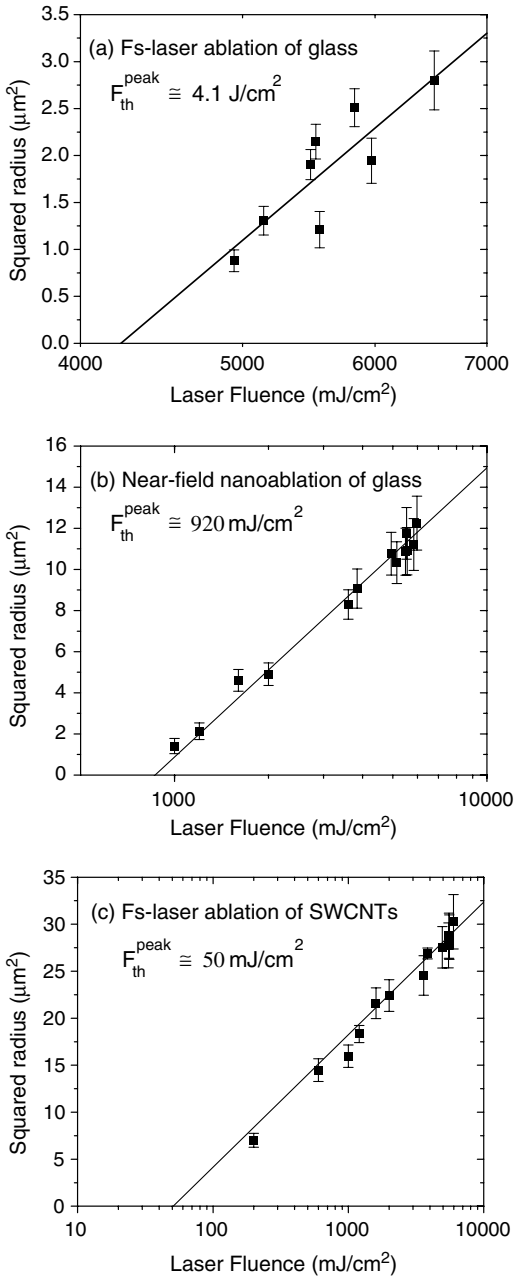

Figure 5. (*a*) Single-shot fs-laser ablation of glass, (*b*) nanoablation of glass and (*c*) fs-laser ablation of SWCNT bundles. The plots show the linear relation between the squared radius of the areas (circles Nos 1, 2 and 3) and the logarithmic of the local laser fluence in accordance with equation (5). The extrapolations to zero provide the single pulse thresholds. The error bars represent the uncertainty of the radius measurement.

threshold for fs-laser ablation of glass (4.1 J cm^{-2}) [1]. We may attribute this nanoablation phenomenon to a possible local-field enhancement near the carbon nanotube bundles. We have previously showed that the near-field enhancement of fs-laser pulses can be used to overcome the diffraction limit of traditional laser ablation for patterning silicon at the nanoscale using gold nanoparticles [34]. Enhancement of electromagnetic fields near the surface of nanoparticles is a result of the excitation of localized surface plasmons as well as the lightning rod effect in metallic nanostructures [35]. Surface plasmons are collections of electrons that oscillate at the interface between the metal and its surrounding dielectric material.

A number of experimental studies detected surface plasmons in multi-wall carbon nanotubes (MWCNTs) [36,37], bundles of SWCNTs [38] and purified SWCNTs [39] using electron energy loss spectroscopy (EELS). These studies showed two main peaks identified as surface plasmons in the ranges 5–7.5 eV and 21–27 eV. Careful EELS measurements by Pitchler *et al* showed some additional peaks at energies below 3.5 eV [39]. Bose [40] later attributed these peaks to possible surface plasmons related to the collective azimuthal motion of electrons on the surface of the nanotubes. More recent experiments demonstrated the nanoantenna operation of MWCNTs [41, 42] as well as their photon coupling capacity (near 2.3 eV) using a fluorescent microbead detection [43].

Despite these studies providing some insight into the plasmonic features of carbon nanotubes, our present understanding of their collective electronic excitation modes or plasmons is still limited. in particular, considering the mixed metallic and semiconducting nature of SWCNT bundles, further studies are needed to elucidate the exact nature of the near-field enhancement phenomena observed in this study.

5. Conclusions

We studied the properties of fs-laser ablation of SWCNTs. We found that the peak fluence threshold for ablation of SWCNTs in a bundle state is 50 mJ cm^{-2}. This value is 5–10 times smaller than the measured fs-laser ablation threshold for graphite and 10 times smaller than that calculated for the ablation of single nanotubes. At a peak laser fluence of 920 mJ cm^{-2}, we observed nanoablation of glass directly beneath the bundled SWCNTs and creation of micrometres long nanolines. The nanoablations are believed to be due to near-field enhancement of the electric field near the bundled SWCNTs. This enhancement by carbon nanotubes could potentially be used in a number of applications. It could possibly be used for lithographic patterning on various materials for electronic as well as for biological applications. Recently, Chen *et al* developed a new technique to interface biocompatible CNTs with a cell surface by carbohydrate-receptor interactions: the modified CNTs are nontoxic and bind to specific sites on cell surfaces [44]. Through this method it might be possible to use the near-field enhancement of SWCNTs to kill cancer cells by irradiating SWCNT labelled cancer cells with ultrafast laser pulses. The advantage of the near-field enhancement is that it only damages atto-litre volumes around the SWCNTs. In addition to the nanoscale localization of laser pulses the nonthermal nature of fs-laser ablation can be exploited to minimize the destruction of surrounding healthy cells.

Acknowledgments

The authors acknowledge the partial funding of this research by the National Science Foundation Grant BES-0508266, State of Texas Advanced Research Initiative and Research Grants of University of Texas at Austin.

References

[1] Ben-Yakar A and Byer R L 2004 Femtosecond laser ablation properties of borosilicate glass *J. Appl. Phys.* **96** 5316–23

[2] Loesel F H, Fischer J P, Gotz M H, Horvath C, Juhasz T, Noack F, Suhm N and Bille J F 1998 Non-thermal ablation of neural tissue with femtosecond laser pulses *Appl. Phys. B—Lasers Opt.* **66** 121–8

[3] Choi T Y and Grigoropoulos C P 2002 Plasma and ablation dynamics in ultrafast laser processing of crystalline silicon *J. Appl. Phys.* **92** 4918–25

[4] Perry M D, Stuart B C, Banks P S, Feit M D, Yanovsky V and Rubenchik A M 1999 Ultrashort-pulse laser machining of dielectric materials *J. Appl. Phys.* **85** 6803–10

[5] Vogel A, Noack J, Huttman G and Paltauf G 2005 Mechanisms of femtosecond laser nanosurgery of cells and tissues *Appl. Phys. B—Lasers Opt.* **81** 1015–47

[6] Deheer W A, Chatelain A and Ugarte D 1995 A carbon nanotube field-emission electron source *Science* **270** 1179–80

[7] Kong J, Franklin N R, Zhou C W, Chapline M G, Peng S, Cho K J and Dai H J 2000 Nanotube molecular wires as chemical sensors *Science* **287** 622–5

[8] Baughman R H, Zakhidov A A and de Heer W A 2002 Carbon nanotubes—the route toward applications *Science* **297** 787–92

[9] Keren K, Berman R S, Buchstab E, Sivan U and Braun E 2003 DNA-templated carbon nanotube field-effect transistor *Science* **302** 1380–2

[10] Gao H J, Kong Y, Cui D X and Ozkan C S 2003 Spontaneous insertion of DNA oligonucleotides into carbon nanotubes *Nano Lett.* **3** 471–3

[11] Besteman K, Lee J O, Wiertz F G M, Heering H A and Dekker C 2003 Enzyme-coated carbon nanotubes as single-molecule biosensors *Nano Lett.* **3** 727–30

[12] Panchapakesan B L, Sivakumar K,Teker K, Cesarone G and Wickstrom E 2005 *Nanobiotechnology* **1** 133–9

[13] Liu Z, Cai W B, He L N, Nakayama N, Chen K, Sun X M, Chen X Y and Dai H J 2007 In vivo biodistribution and highly efficient tumour targeting of carbon nanotubes in mice *Nature Nanotechnol.* **2** 47–52

[14] Kam N W S, O'Connell M, Wisdom J A and Dai H J 2005 Carbon nanotubes as multifunctional biological transporters and near-infrared agents for selective cancer cell destruction *Proc. Natl Acad. Sci. USA* **102** 11600–5

[15] Link S and El-Sayed M A 1999 Spectral properties and relaxation dynamics of surface plasmon electronic oscillations in gold and silver nanodots and nanorods *J. Phys. Chem.* B **103** 8410–26

[16] Oldenburg S J, Averitt R D, Westcott S L and Halas N J 1998 Nanoengineering of optical resonances *Chem. Phys. Lett.* **288** 243–7

[17] Huang X H, El-Sayed I H, Qian W and El-Sayed M A 2006 Cancer cell imaging and photothermal therapy in the near-infrared region by using gold nanorods *J. Am. Chem. Soc.* **128** 2115–20

[18] Loo C, Lowery A, Halas N, West J and Drezek R 2005 Immunotargeted nanoshells for integrated cancer imaging and therapy *Nano Lett.* **5** 709–11

[19] El-Sayed I H, Huang X H and El-Sayed M A 2006 Selective laser photo-thermal therapy of epithelial carcinoma using anti-EGFR antibody conjugated gold nanoparticles *Cancer Lett.* **239** 129–35

[20] Reitze D H, Wang X, Ahn H and Downer M C 1989 Femtosecond Laser melting of graphite *Phys. Rev.* B **40** 11986–9

[21] Preuss S and Stuke M 1995 Subpicosecond ultraviolet-laser ablation of diamond - nonlinear properties at 248 Nm and time-resolved characterization of ablation dynamics *Appl. Phys. Lett.* **67** 338–40

[22] Lenner M, Kaplan A and Palmer R E 2007 Nanoscopic Coulomb explosion in ultrafast graphite ablation *Appl. Phys. Lett.* **90** 153119

[23] Jeschke H O and Garcia M E 2002 Theoretical description of the ultrafast ablation of diamond and graphite: dependence of thresholds on pulse duration *Appl. Surf. Sci.* **197** 107–13

[24] Jeschke H O, Garcia M E and Bennemann K H 2001 Theory for the ultrafast ablation of graphite films *Phys. Rev. Lett.* **87** 015003

[25] Corio P, Santos P S, Pimenta M A and Dresselhaus M S 2002 Evolution of the molecular structure of metallic and semiconducting carbon nanotubes under laser irradiation *Chem. Phys. Lett.* **360** 557–64

[26] Ma R Z, Wei B Q, Xu C L, Liang J and Wu D H 2000 The morphology changes of carbon nanotubes under laser irradiation *Carbon* **38** 636–8

[27] Romero A H, Garcia M E, Valencia F, Terrones H, Terrones M and Jeschke H O 2005 Femtosecond laser nanosurgery of defects in carbon nanotubes *Nano Lett.* **5** 1361–5

[28] Dumitrica T, Garcia M E, Jeschke H O and Yakobson B I 2006 Breathing coherent phonons and caps fragmentation in carbon nanotubes following ultrafast laser pulses *Phys. Rev.* B **74** 193406

[29] Kocabas C, Meitl M A, Gaur A, Shim M and Rogers J A 2004 Aligned arrays of single-walled carbon nanotubes generated from random networks by orientationally selective laser ablation *Nano Lett.* **4** 2421–6

[30] Liu J *et al* 1998 Fullerene pipes *Science* **280** 1253–6

[31] Chen J, Hamon M A, Hu H, Chen Y S, Rao A M, Eklund P C and Haddon R C 1998 Solution properties of single-walled carbon nanotubes *Science* **282** 95–98

[32] Sabba Y and Thomas E L 2004 High-concentration dispersion of single-wall carbon nanotubes *Macromolecules* **37** 4815–20

[33] Sokolowski-Tinten K K, Kudryashov S, Temnov V, Biakowski J, Vonder Linde D, Cavalleri A, Jeschke H O, Garcia M E and Bennemann K H 2000 *Ultrafast Phenomena XII*, *Proc. 12th Int. Conf.* (*Charleston, SC, USA, 9–13 July 2000*), *Springer Series in Chemical Physics* vol 66, ed T Elsaesser *et al* (Berlin: Springer) pp 425–7

[34] Eversole D, Luk'yanchuk B and Ben-Yakar A 2007 Plasmonic laser nanoablation of silicon by the scattering of femtosecond pulses near gold nanospheres *Appl. Phys. A—Mater. Sci. Process.* **89** 283–91

[35] Lal S, Link S and Halas N J 2007 Nano-optics from sensing to waveguiding *Nature Photon.* **1** 641–8

[36] Bursill L A, Stadelmann P A, Peng J L and Prawer S 1994 Surface-plasmon observed for carbon nanotubes *Phys. Rev.* B **49** 2882–7

[37] Bommeli F, Degiorgi L, Wachter P, Bacsa W S, deHeer W A and Forro L 1996 Evidence of anisotropic metallic behaviour in the optical properties of carbon nanotubes *Solid State Commun.* **99** 513–7

[38] Kuzuo R, Terauchi M, Tanaka M and Saito Y 1994 Electron-energy-loss spectra of single-shell carbon nanotubes *Japan. J. Appl. Phys. Part 2—Lett.* **33** L1316–19

[39] Pichler T, Knupfer M, Golden M S, Fink J, Rinzler A and Smalley R E 1998 Localized and delocalized electronic states in single-wall carbon nanotubes *Phys. Rev. Lett.* **80** 4729–32

[40] Bose S M 2001 Low energy plasmon peaks in the electron energy loss spectra of single-wall carbon nanotubes *Phys. Lett.* A **289** 255–6

[41] Rybczynski J, Kempa K, Herczynski A, Wang Y, Naughton M J, Ren Z F, Huang Z P, Cai D and Giersig M

2007 Subwavelength waveguide for visible light *Appl. Phys. Lett.* **90** 021104

[42] Wang Y, Kempa K, Kimball B, Carlson J B, Benham G, Li W Z, Kempa T, Rybczynski J, Herczynski A and Ren Z F 2004 Receiving and transmitting light-like radio waves: antenna effect in arrays of aligned carbon nanotubes *Appl. Phys. Lett.* **85** 2607–9

[43] Lu Q, Rao R, Sadanadan B, Que W, Rao A M and Ke P C 2005 Coupling of photon energy via a multiwalled carbon nanotube array *Appl. Phys. Lett.* **87** 173102

[44] Chen X, Tam U C, Czlapinski J L, Lee G S, Rabuka D, Zettl A and Bertozzi C R 2006 Interfacing carbon nanotubes with living cells *J. Am. Chem. Soc.* **128** 6292–3